Data Depository: Additional Examples of EDXRF Spectra

Herzog F.A., 2015. The potential of a portable EDXRF spectrometer for gemmology. *Journal of Gemmology*, **34**(5), pp. 404–418.
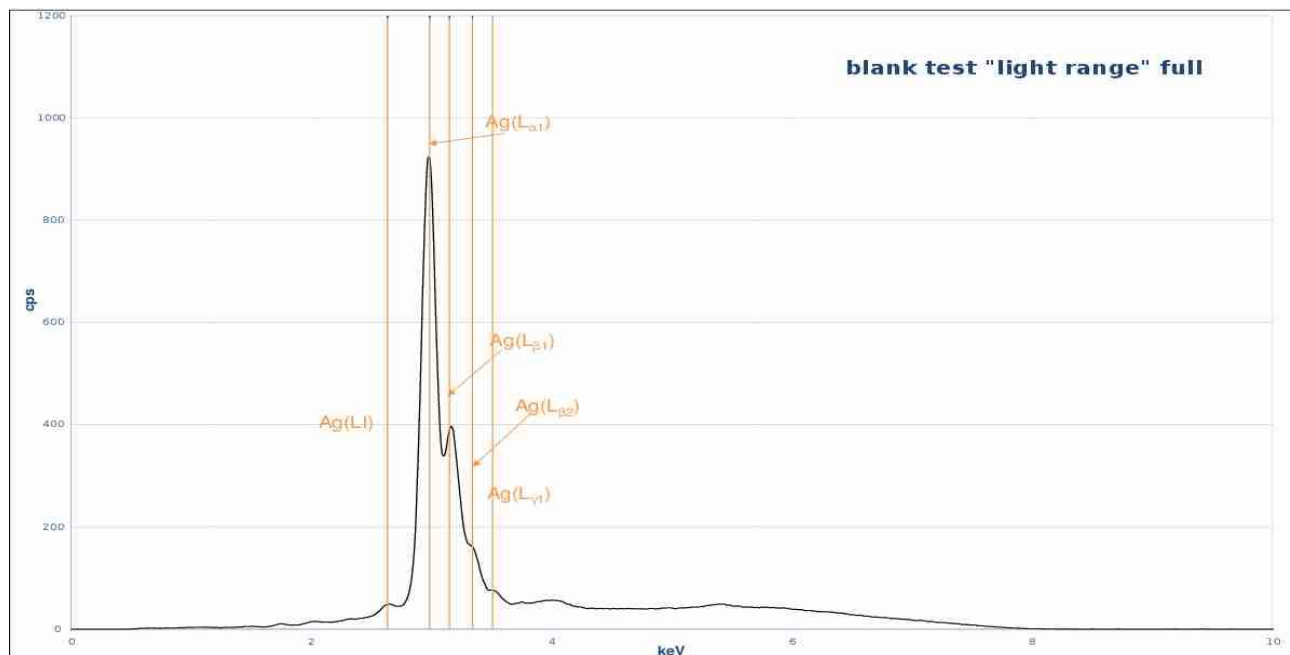
System Peaks

Figure DD-1: Full 'light range' spectrum of a blank test, including the punched (4 mm diameter) polyethylene sheet of 0.1 mm thickness. Here the system peaks are purely dictated by the X-ray tube's anode material (Ag). In this range there is no primary filter to reduce these signals. These peaks are usually no problem for interpreting the 'light range' spectra—the only overlap concerns the Ag(LI) line with the Cl(K_α) line. The usual Ar peaks from the air surrounding the sample holder (and hence also system peaks) are completely covered by the Ag peaks.
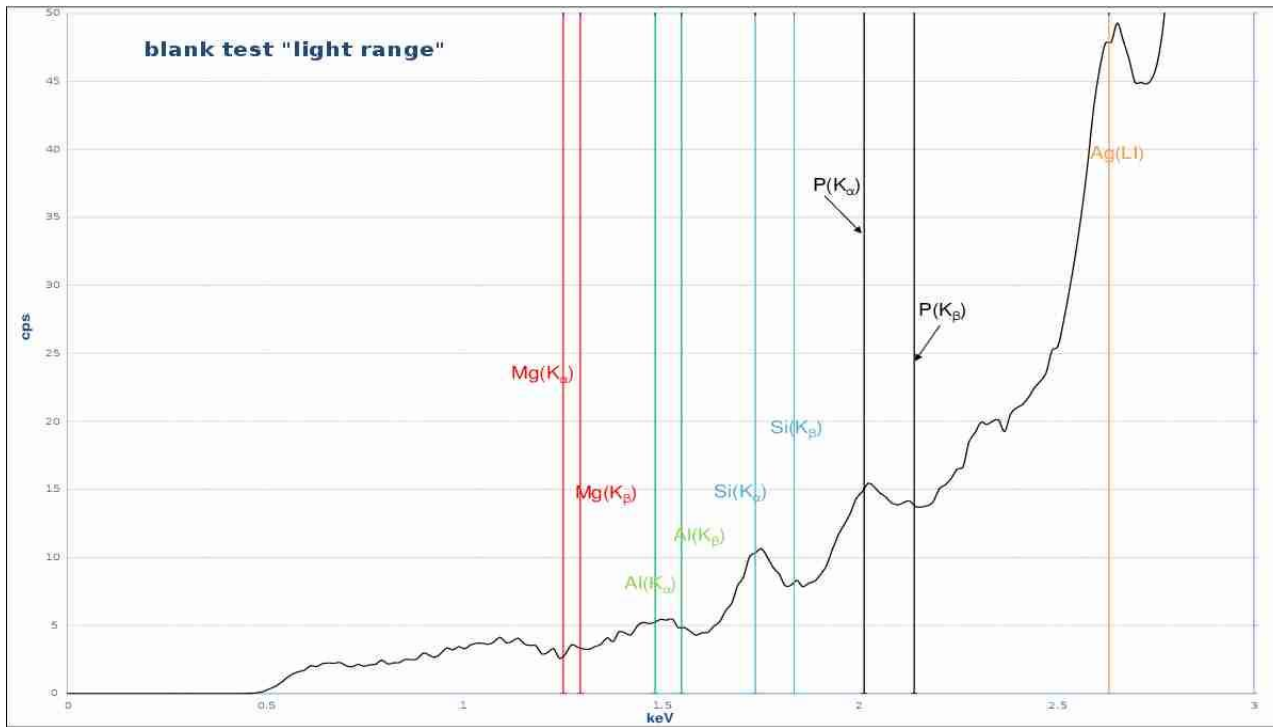
Figure DD-2: 'Light range' spectrum as in Figure DD-1 but zoomed to the range of interest for the detection of light elements (see Table II). The bumpy structure in the area from Mg to S was not problematic, only the Ag(LI) is very close to the Cl line, as mentioned above.
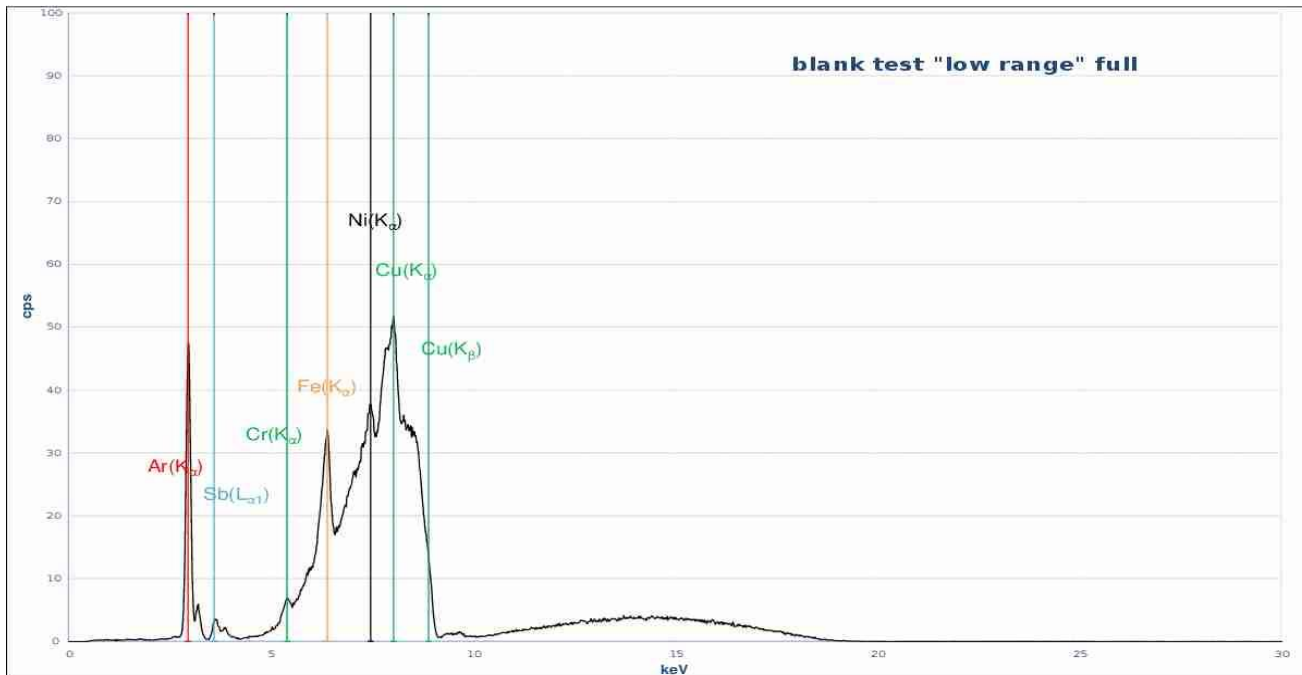

Figure DD-3: Full 'low range' spectrum, showing peaks that are dominated by Ni and Cu. The filter used in this excitation range reportedly consists of Cu, but this spectrum suggests that it is composed of Ni and Cu since the Cu(K_β) is strongly absorbed, which is typically achieved with a Ni filter. The Ar is a system peak from the air surrounding the sample holder. The Fe peak must have its origin along the emerging beam, as well as the small Cr peak. The Sb peak is a remnant of the production process of the polyethylene sheet: These sheets are fed over Sb-containing rollers during the production process (Sb is soft and thus the sheets do not get scratched).
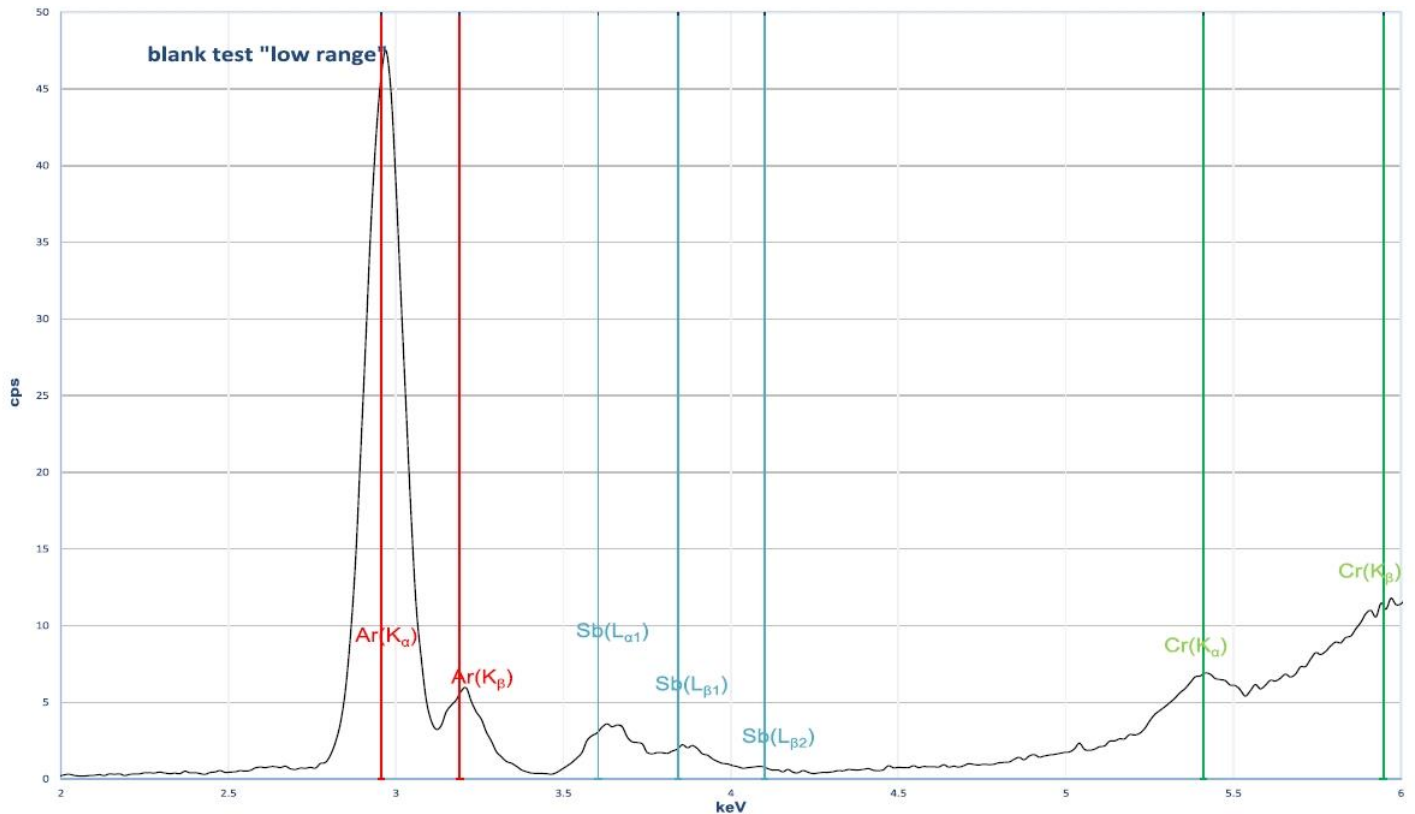
Figure DD-4: 'Low range' spectrum zoomed to the energy range of 2–6 keV, crucial for the detection of the elements K–Cr (K-lines) and Ba–Nd (L-lines). The most significant system peak in this range is the Ar line from the small air volume surrounding the detector. Its signal can be strongly reduced by using a He-purge unit.
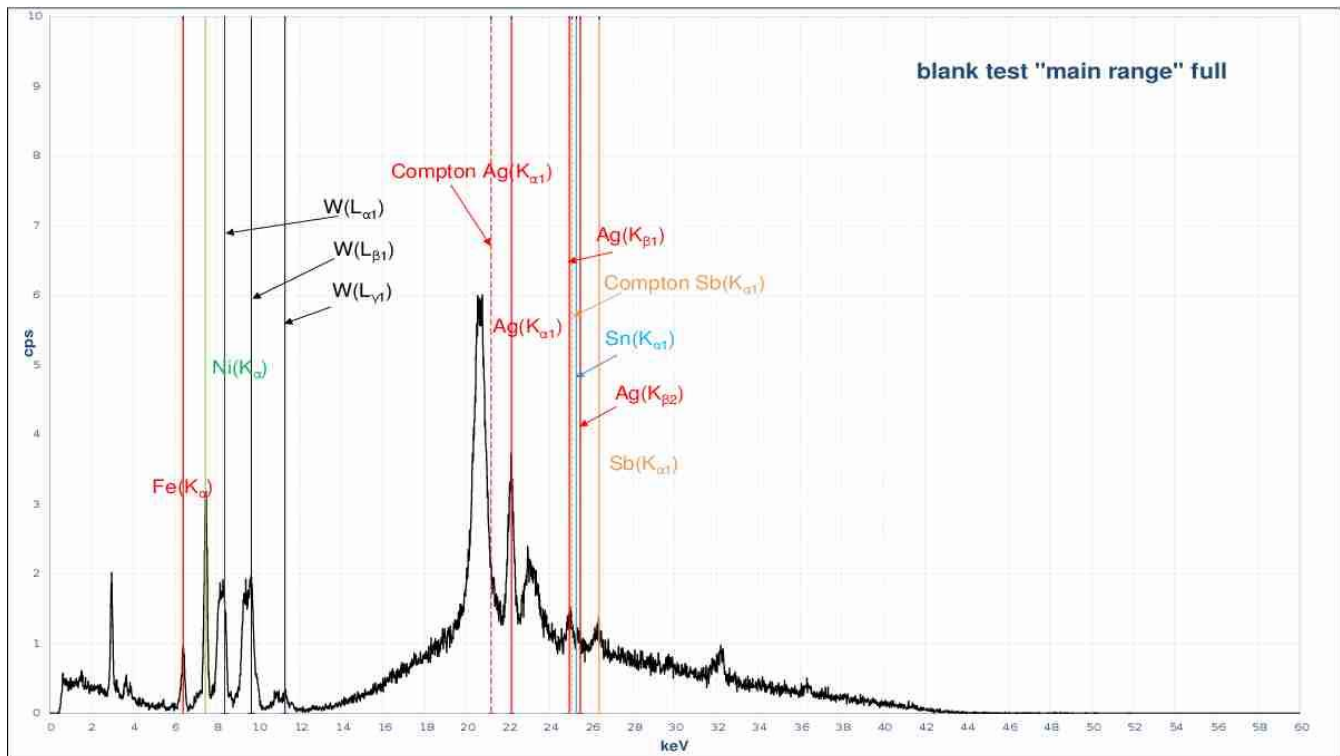

Figure DD-5: 'Main range' spectrum of a blank test. Tungsten (W) originates from the primary excitation beam hitting the collimator material, and Ni receives a contribution from the emerging beam. The low Fe is from a source unknown to the author. The Sn contribution reflects the solder used in the detector. The Sb peak is a remnant of the production process of the polyethylene sheet.
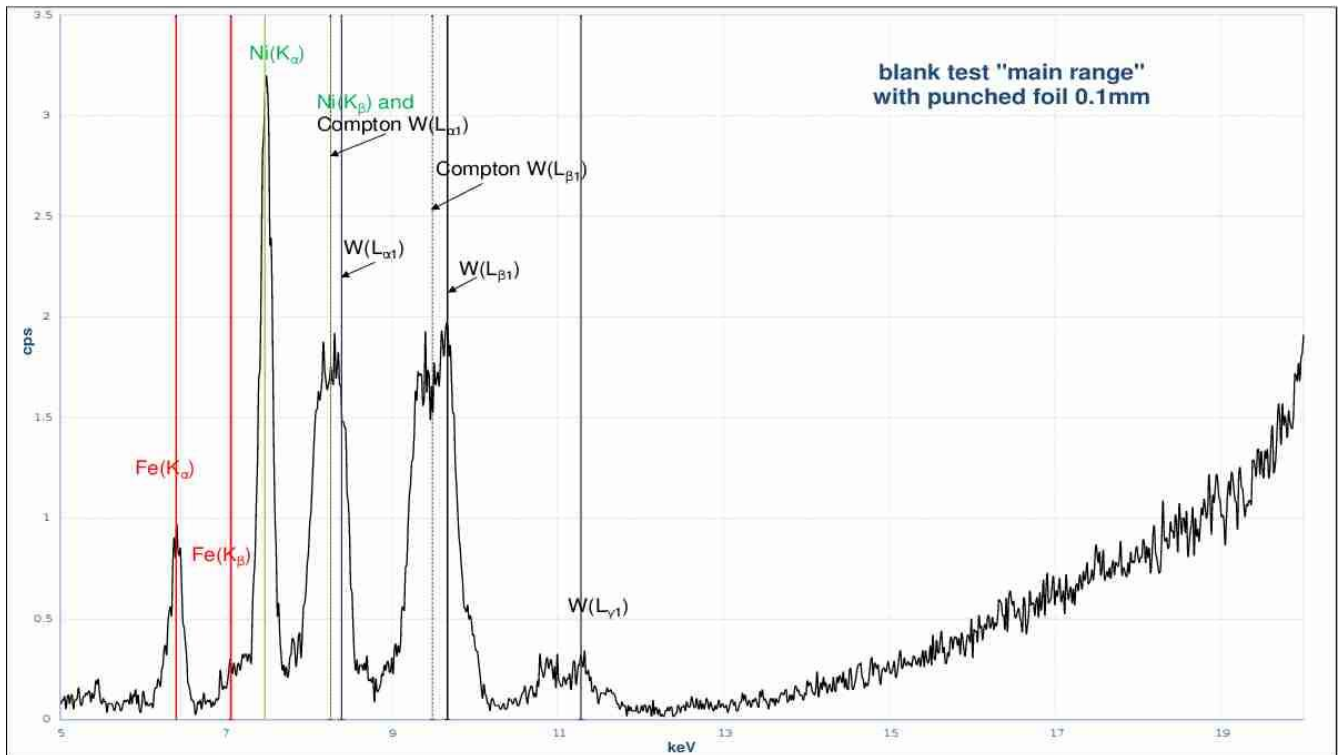
3

Figure DD-6: 'Main range' spectrum as in Figure DD-5, but zoomed to the relevant range to detect the elements Ti–Mo (K-lines) and Ta–Bi (L-lines). The most significant peaks here are due to Fe and Ni. These can be seen in most 'main range' spectra and sometimes they are quite intense. Generally the W peaks get absorbed by the samples itself, so they very rarely disturb the qualitative interpretation.
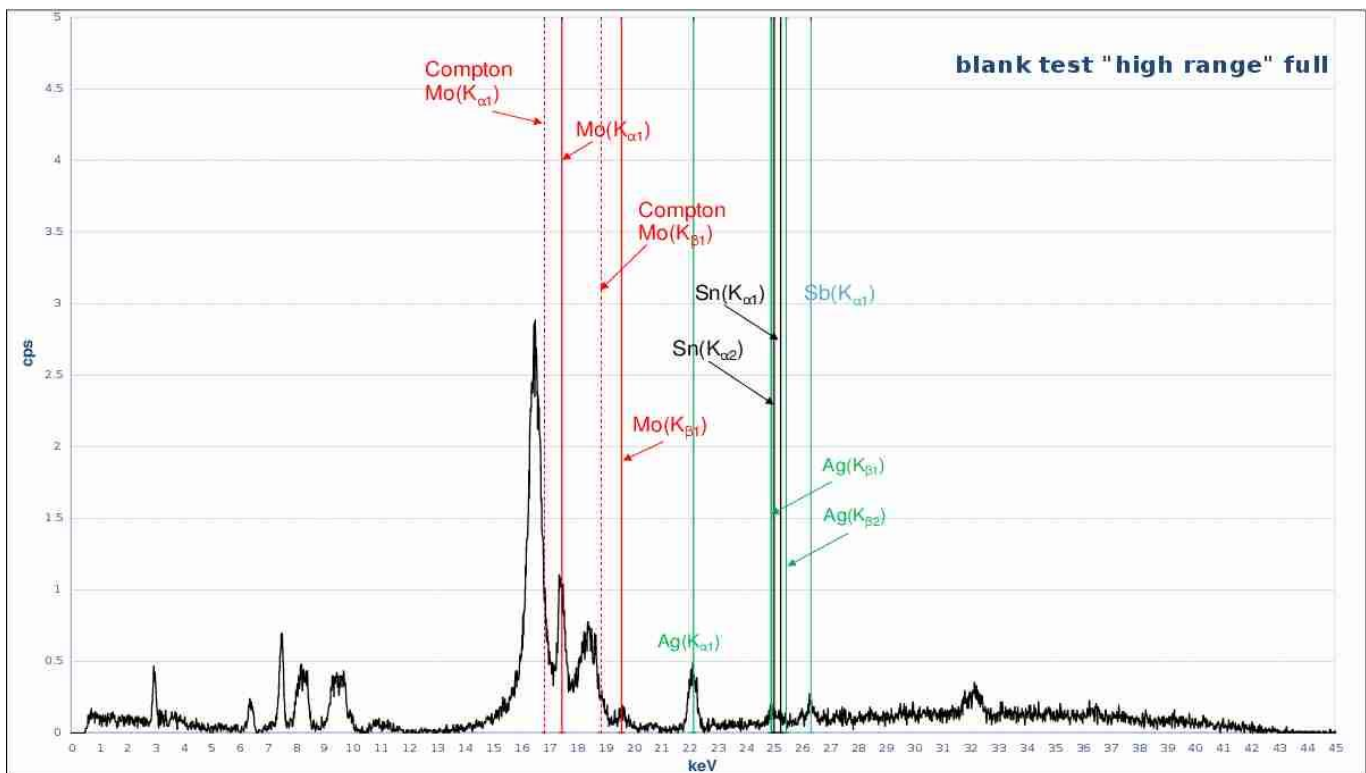

Figure DD-7: 'High range' spectrum of a blank test. This spectrum is dominated by Mo peaks from the primary filter. Otherwise, as the excitation energy is the same as for the 'main range', the peaks seen in that spectrum also appear here (L-peaks due to W in the 6 keV region) as well as the solder peaks (Sn) and the Ag peak from the X-ray tube.
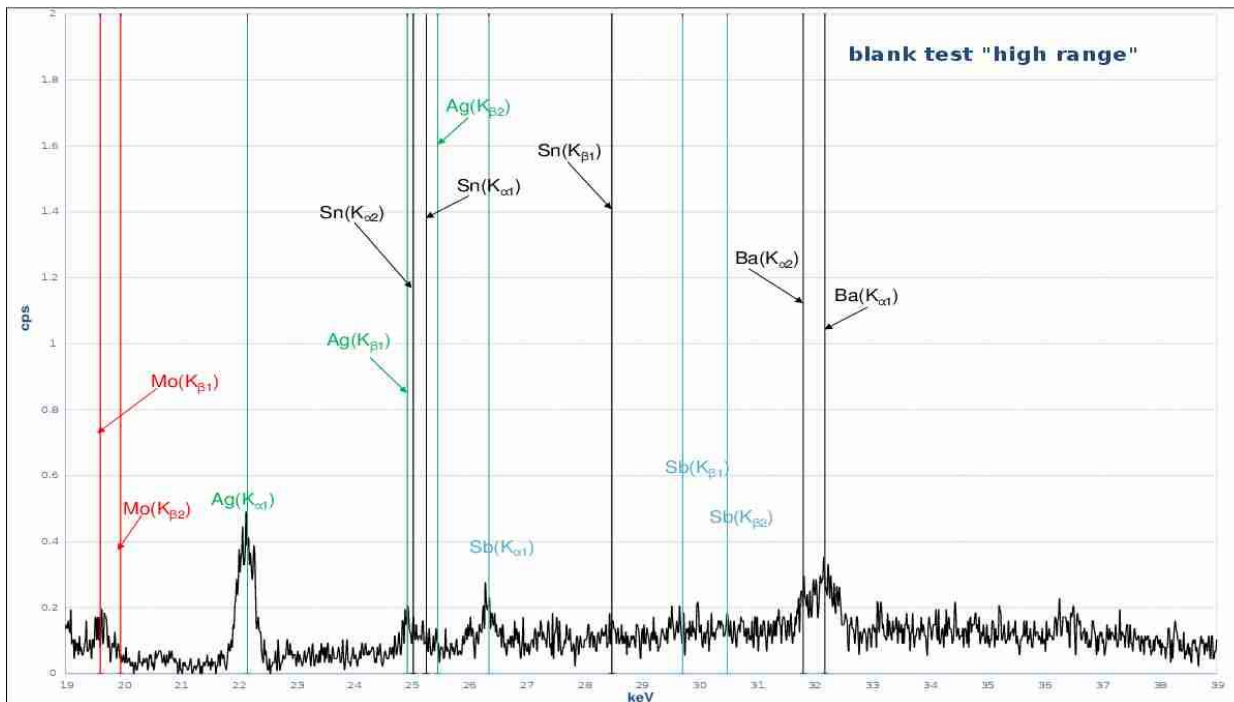
4

Figure DD-8: 'High range' spectrum as seen in Figure DD-7, but zoomed to the energy range 19–39 keV to see the elements Rh–Nd. The intensity of the background from these system peaks is very low and was never a significant factor within this analysis.
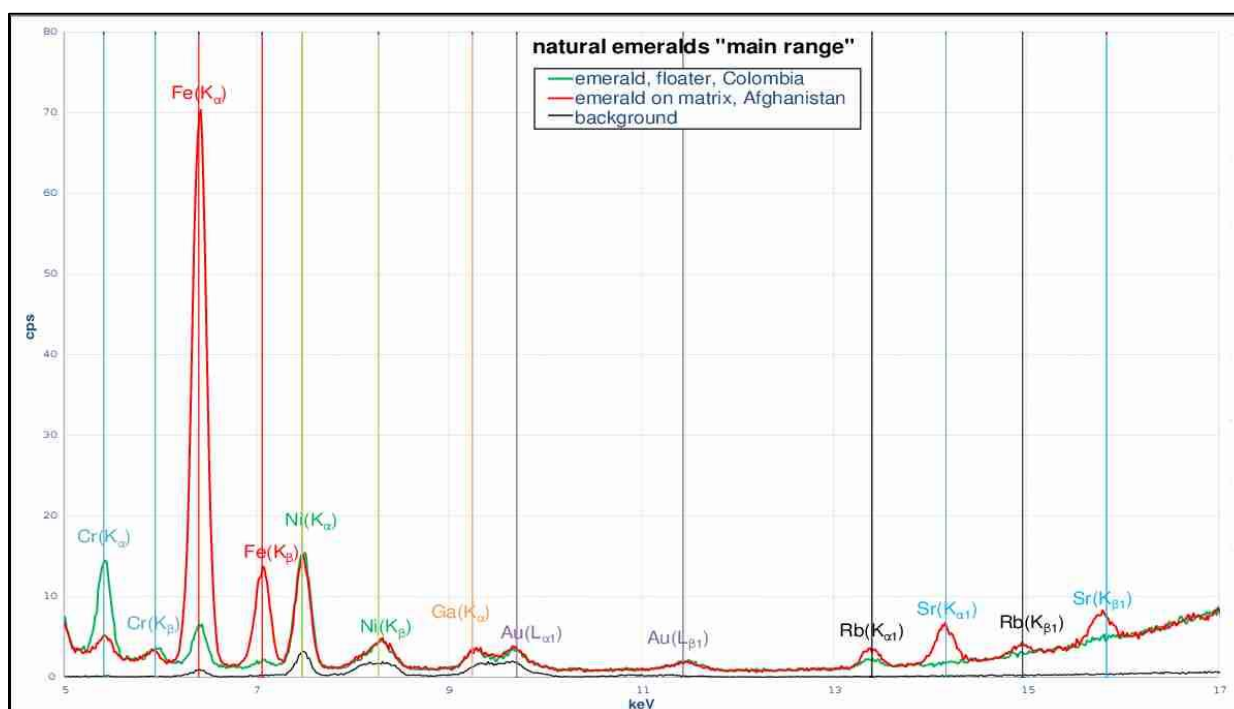
Emerald

Figure DD-9: 'Main range' spectra of natural emeralds. The spectra of both samples coincide in the area of the system peaks (Ni, W, Au) and their matrix seems to enhance their effect, but the numerical result for these concentrations was 'LOD' for these elements. These spectra clearly show that the emerald from Afghanistan (sample 11) contains much more Fe than the Colombian emerald (sample 10). This Colombian crystal also has a higher Cr content and lower alkaline and alkaline-earth contents.
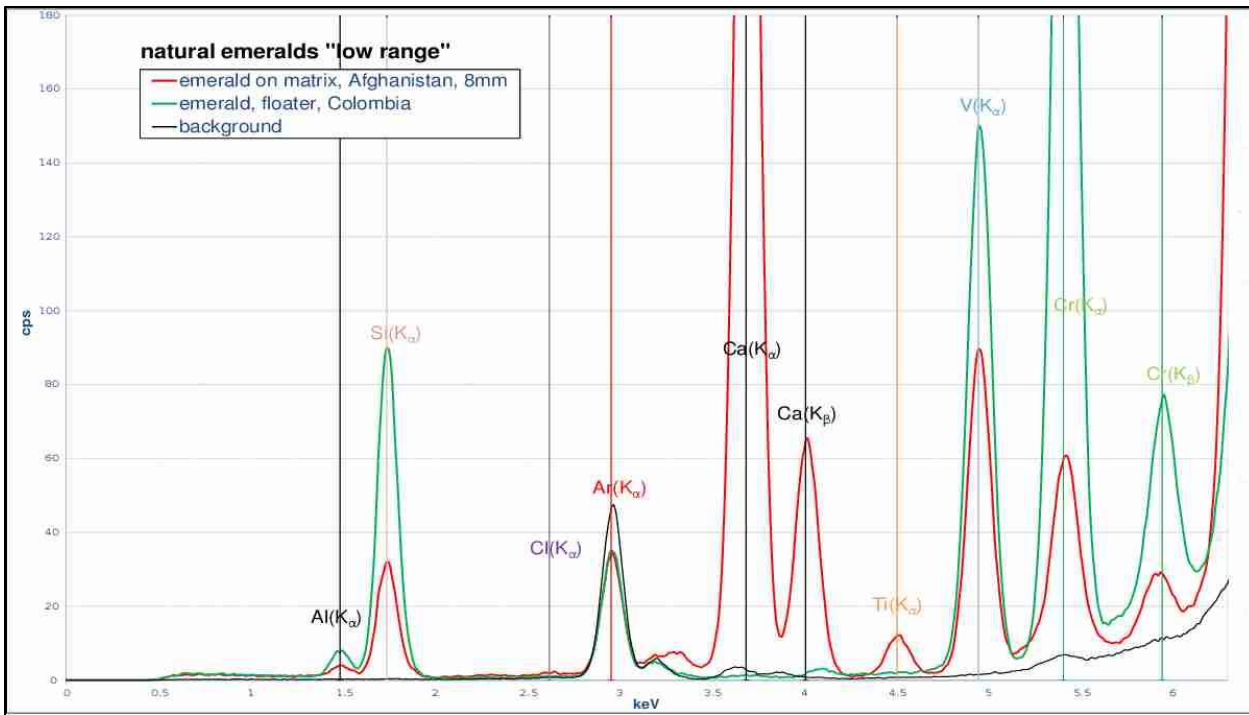
5

Figure DD-10: 'Low range' spectra of natural emeralds. Both the Colombian (sample 10) and Afghan (sample 11) emeralds contain V as the green chromophore. The Ca peaks for (sample 11) are due to the matrix (both spectra were recorded with the 8 mm collimator). By using the 3 mm collimator (~the width of the large crystal) these peaks as well as the Ti peak disappeared and the Sc contribution could be identified.
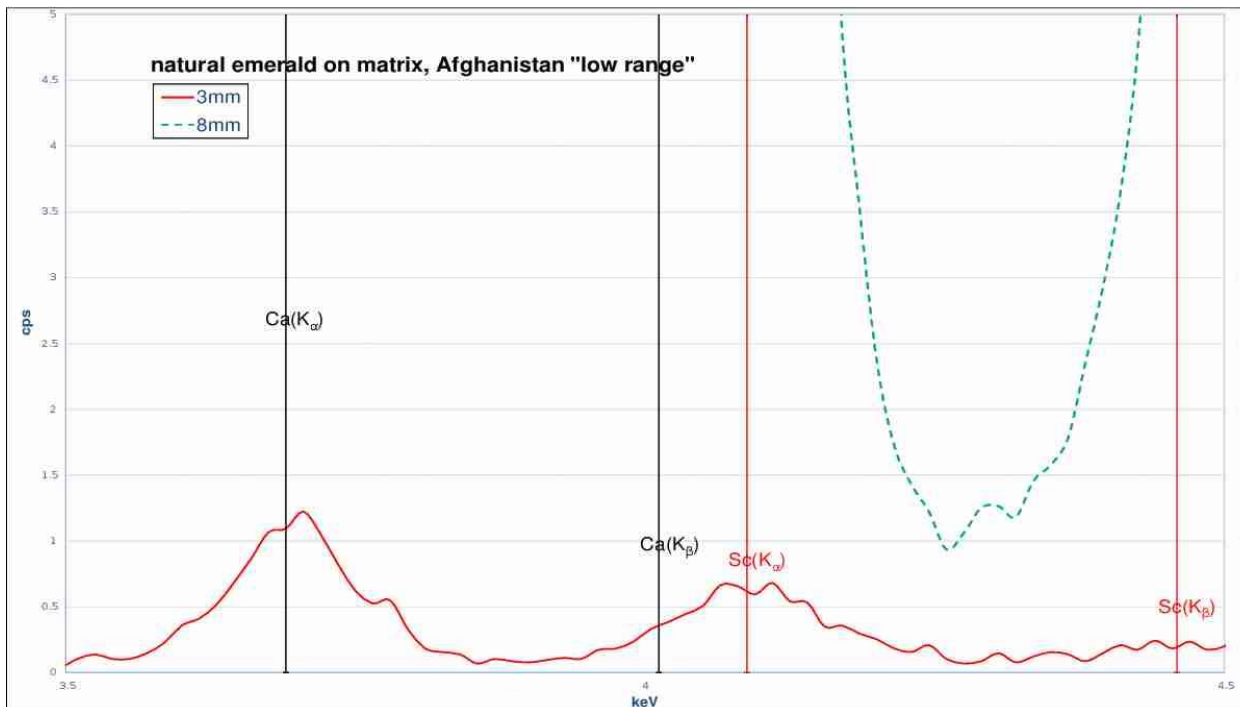

Figure DD-11: 'Low range' spectra of the Afghan emerald (sample 11). The green curve was recorded with the 8 mm collimator, and due to the calcite in the matrix the Ca peaks are very dominant. The 3 mm collimator enables a better analysis of the emerald. The signal for Sc can barely be detected; by increasing the measuring time for the 'low range' from 120 sec to a longer time the signal can be improved.
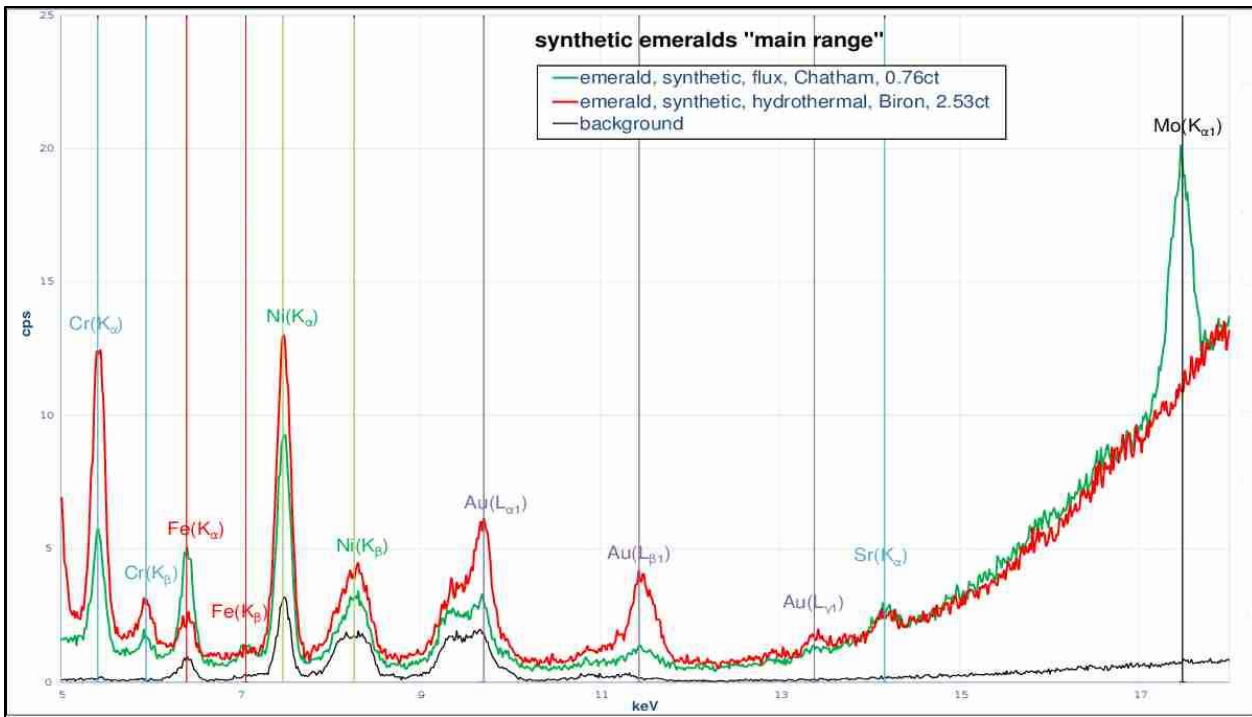
Figure DD-12: 'Main range' spectra of the synthetic emeralds. The Mo flux residue in the Chatham gem (13) is a clear indication of its synthesis process. There is no additional evidence of synthesis within this energy range, except maybe the low Fe content, as many natural emeralds contain significant iron (except Colombian stones). Although the system peaks of Ni and Au are quite high, their values registered as 'LOD'.
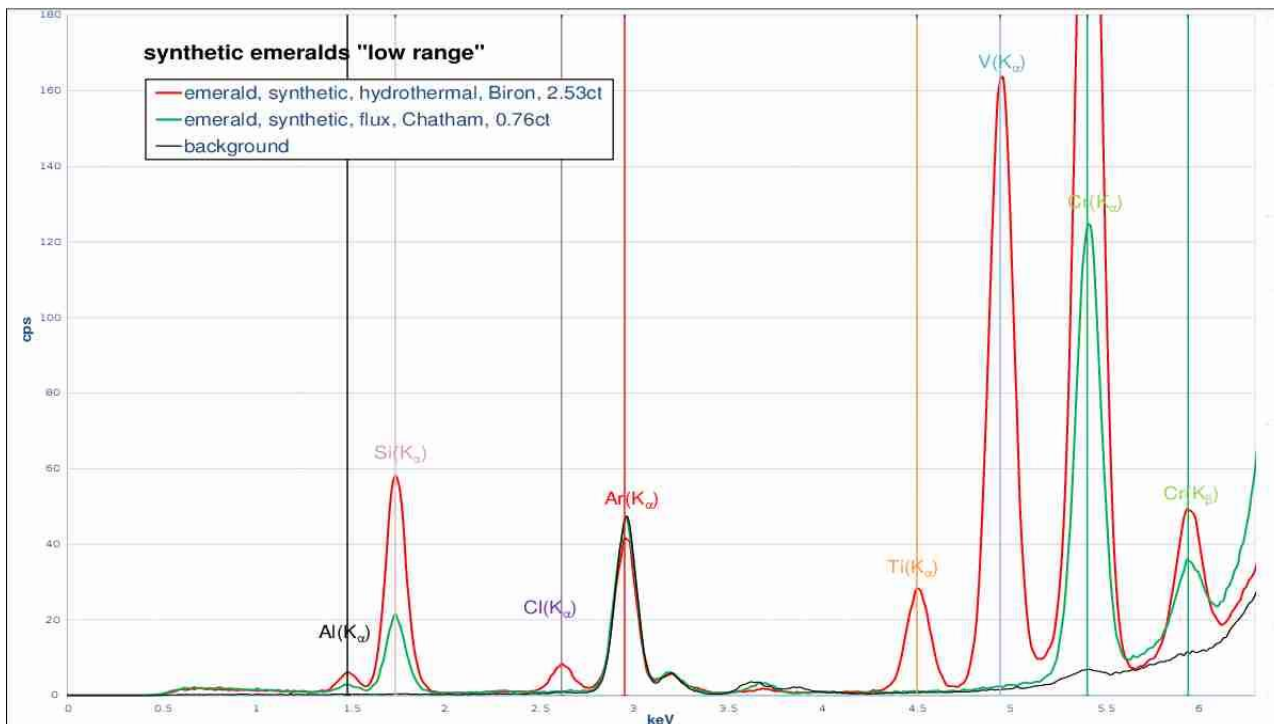

Figure DD-13: 'Low range' spectra of synthetic emeralds. The Cl peak for the Biron synthetic emerald (sample 12) is a clear indicator of its synthetic nature, as HCl is used to bring Cr into solution during the hydrothermal growth process. It is surprising that the V content of the Chatham gem (sample 13) is so low, as the Chatham process, at least in earlier years, was using a V flux component (Nassau, 1980). Note that the $Cl(K_\alpha)$ peak at 2.622 keV is very close to the Ag(LI) peak (2.634 keV). This is no problem if Cl is checked in the 'low range', but it is a problem in the 'light range' spectrum, as in this range there is no filter and the Ag peaks are omnipresent with their L-shell peaks.
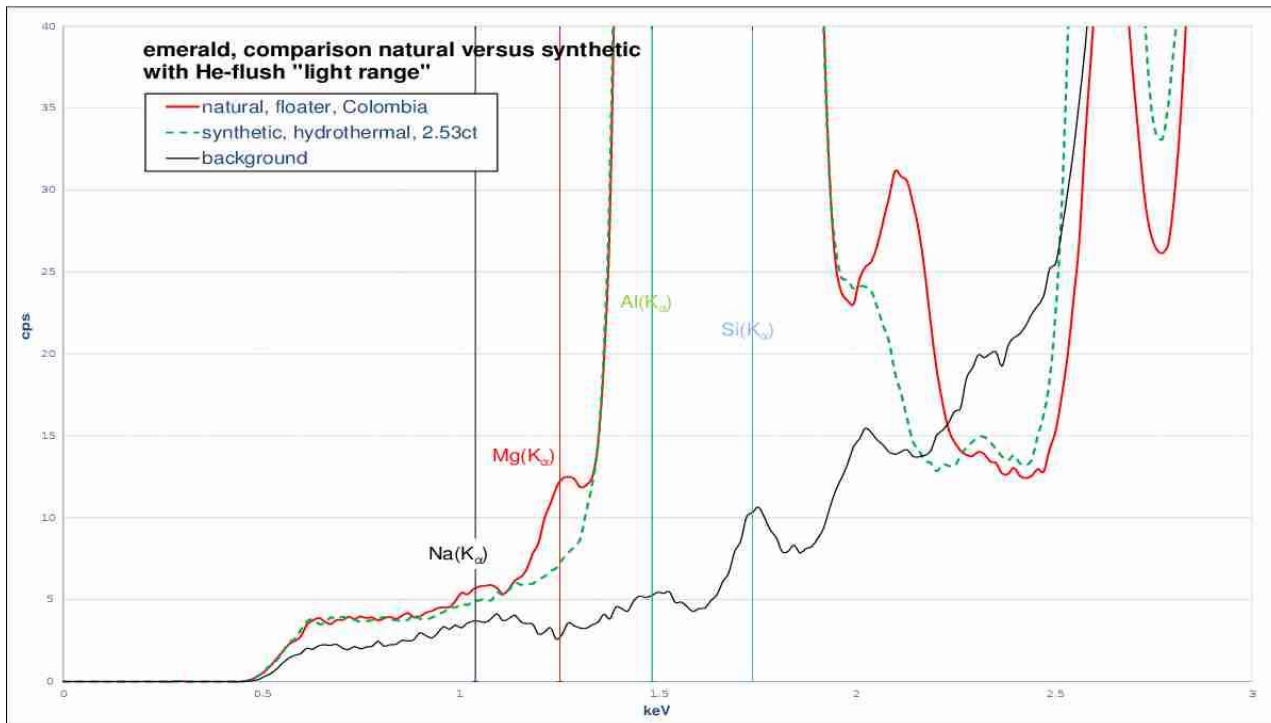
Figure DD-14: Light element differences between synthetic and natural emeralds. Natural emeralds typically contain small amounts of Na and Mg (Hänni, 1982), but not synthetic emeralds. This is shown here for a natural Colombian emerald (sample 10) and a Biron synthetic (sample 12). To do this analysis the He-purge unit must be used. In addition, by extending the measurement time for the 'light range' spectra, the S/N can be improved.
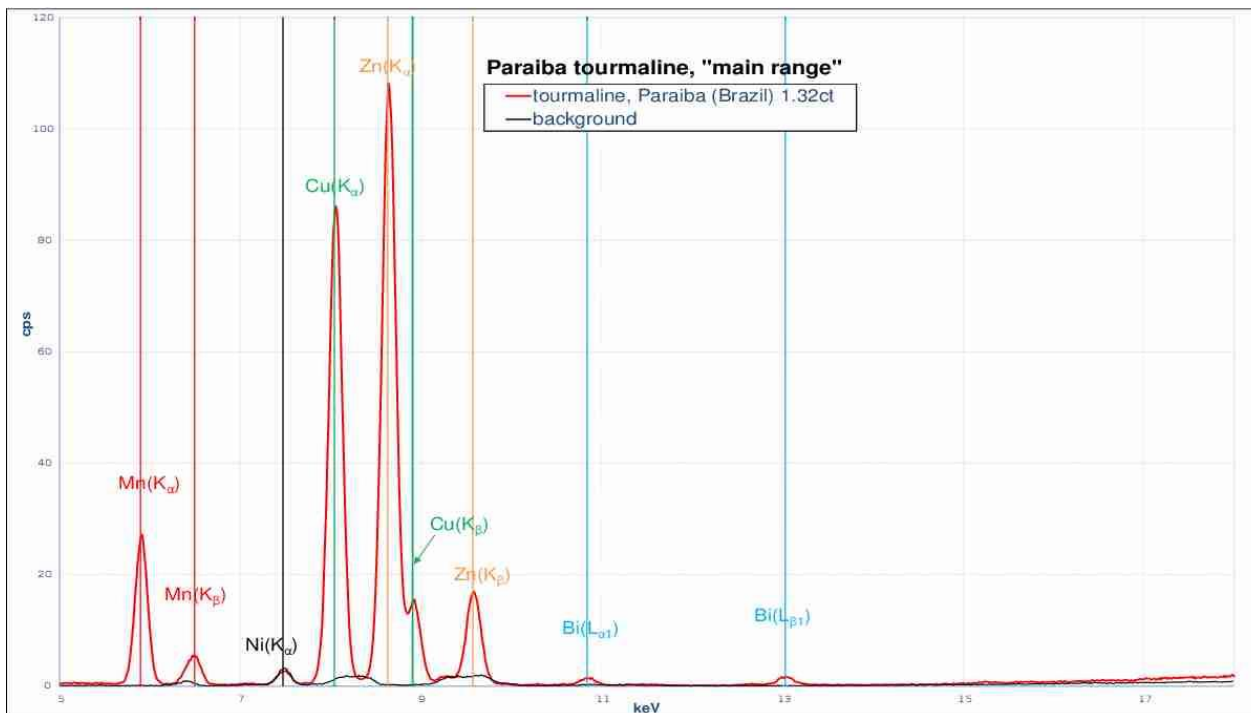
Tourmaline

Figure DD-15: 'Main range' spectrum of a Brazilian Paraíba tourmaline (sample 14). The characteristic Mn and Cu-bearing pattern is obvious. The ratio Cu/Mn >1, the high Zn peak and the moderate Bi component may give indications for a Brazilian origin, although origin determination by qualitative EDXRF analysis for Paraíba-type tourmalines is not rigorous (there are many light elements, not detectable by EDXRF, that are necessary for proper origin determination of these stones).
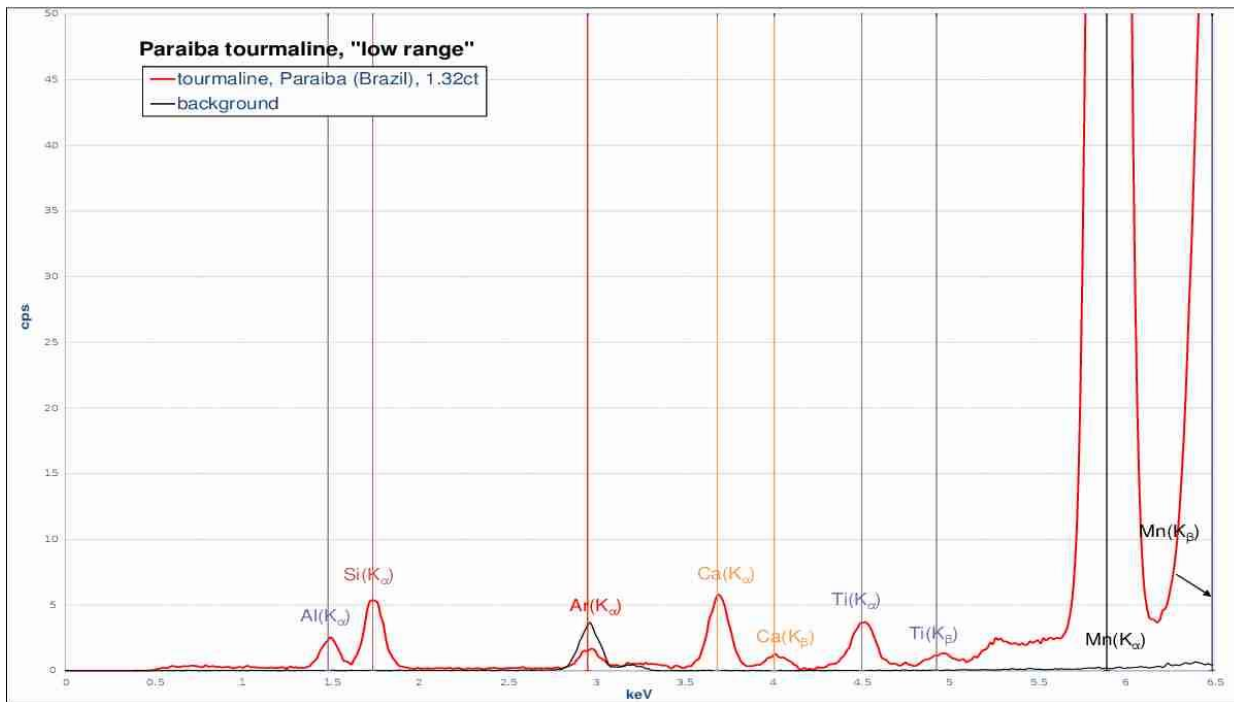
8

Figure DD-16: 'Low range' spectrum of the same stone (sample 14) as in Figure DD-15. It can be seen that this tourmaline has possibly a small liddicoatite component (Ca).
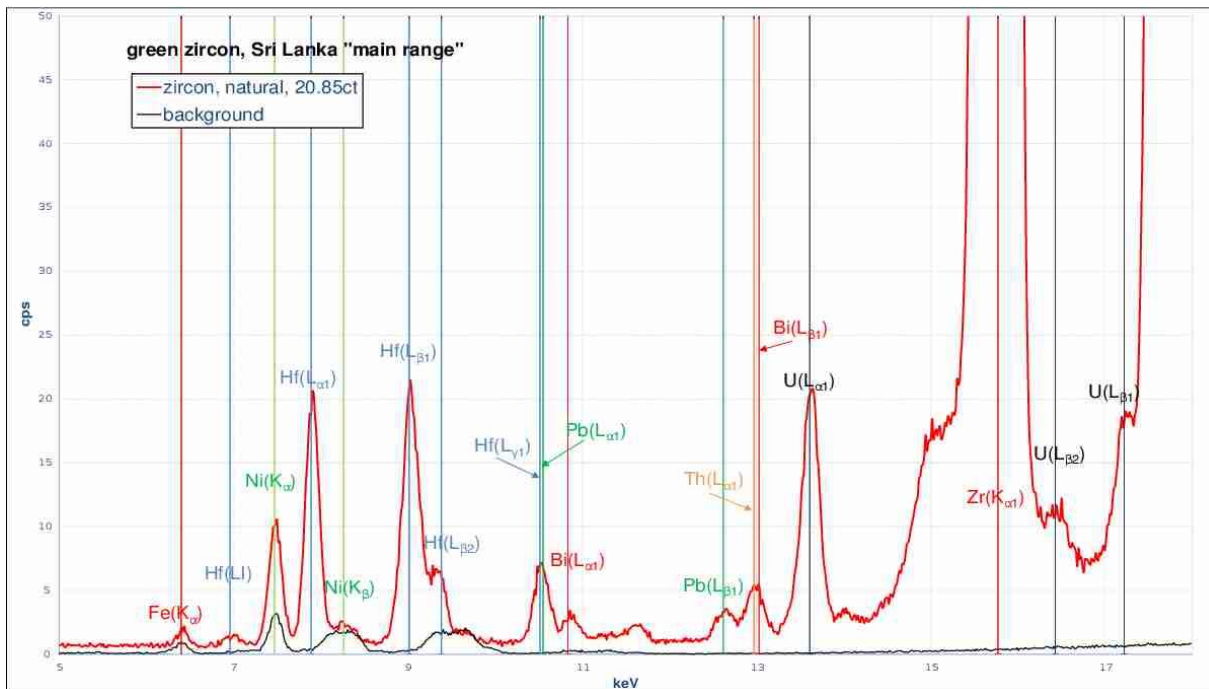
Zircon

Figure DD-17: 'Main range' spectrum of a green, natural zircon from Sri Lanka (sample 15). This spectrum clearly shows that the portable EDXRF analyser can be used for detecting heavy elements. Zr is a main constituent, and therefore the figure has been optimized for the impurities within zircon. Apart from Hf, which is known to be a common companion of Zr, the elements U, Bi and Pb can be identified by at least two peaks—although quite close to the energy resolution limit of the instrument. Only one peak for Th is seen, but a properly calibrated system would be able to de-convolute any peak overlaps.
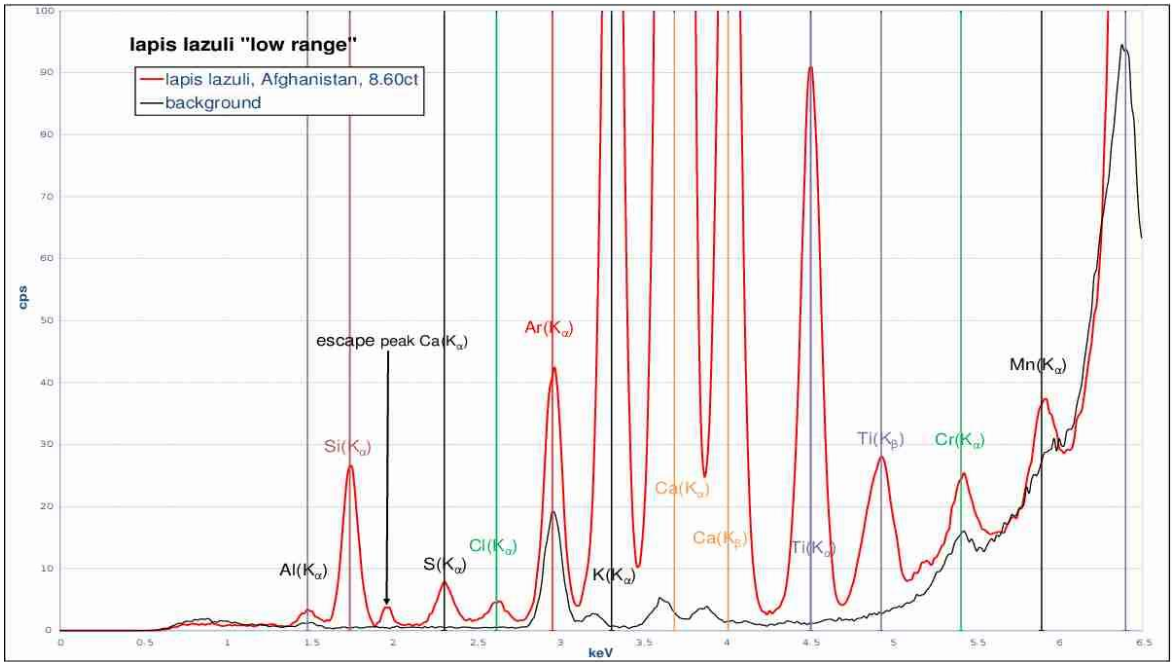
Lapis Lazuli

Figure DD-18: 'Low range' spectrum of a lapis lazuli (sample 16). The light elements S and Cl can clearly be seen in this spectrum, as well as an 'escape peak' from the large Ca content; it originates from the X-ray– fluorescent $Ca(K_\alpha)$ at 3.69 keV producing $Si(K_\alpha)$ fluorescence at 1.74 keV escaping the detector. Therefore, with a Si SDD detector, the 'escape peak' of $Ca(K_\alpha)$ is at 1.95 keV.
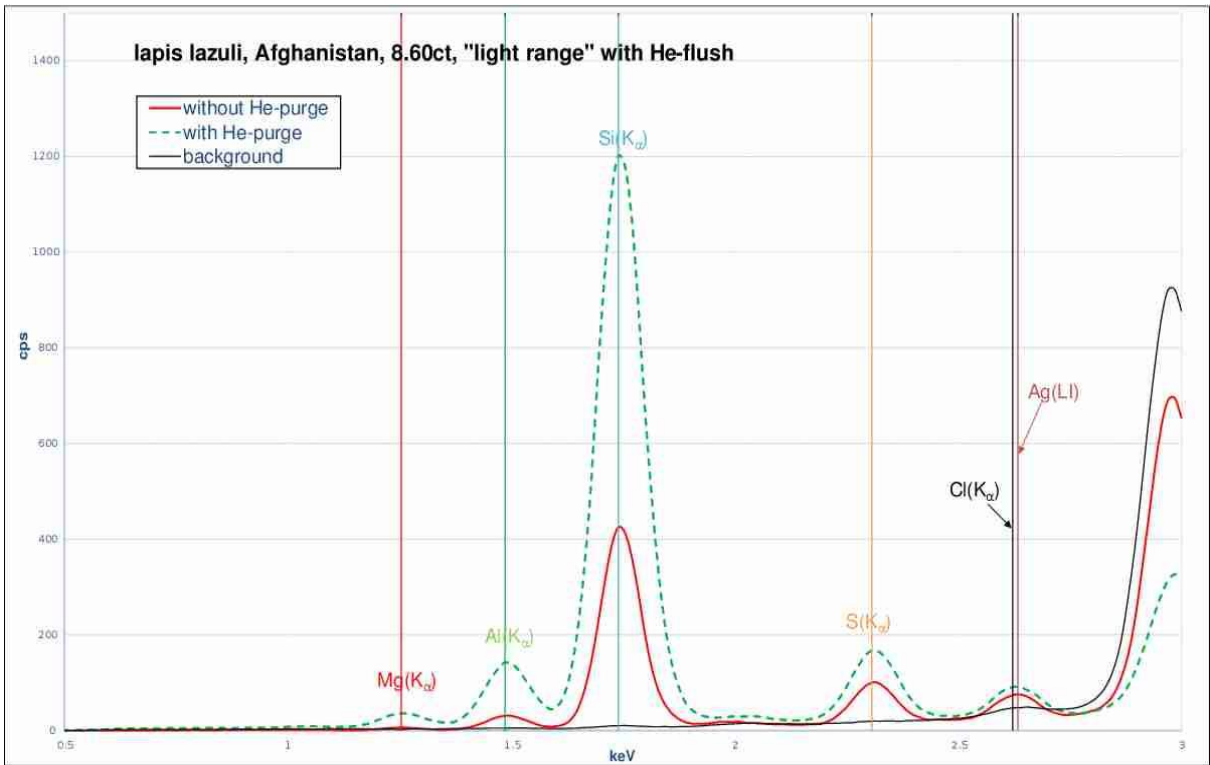

Figure DD-19: 'Light range' spectra of a lapis lazuli (sample 16), recorded with and without the He purge unit. The S and Cl components are clearly visible in both spectra, as already suggested by Figure DD-18.
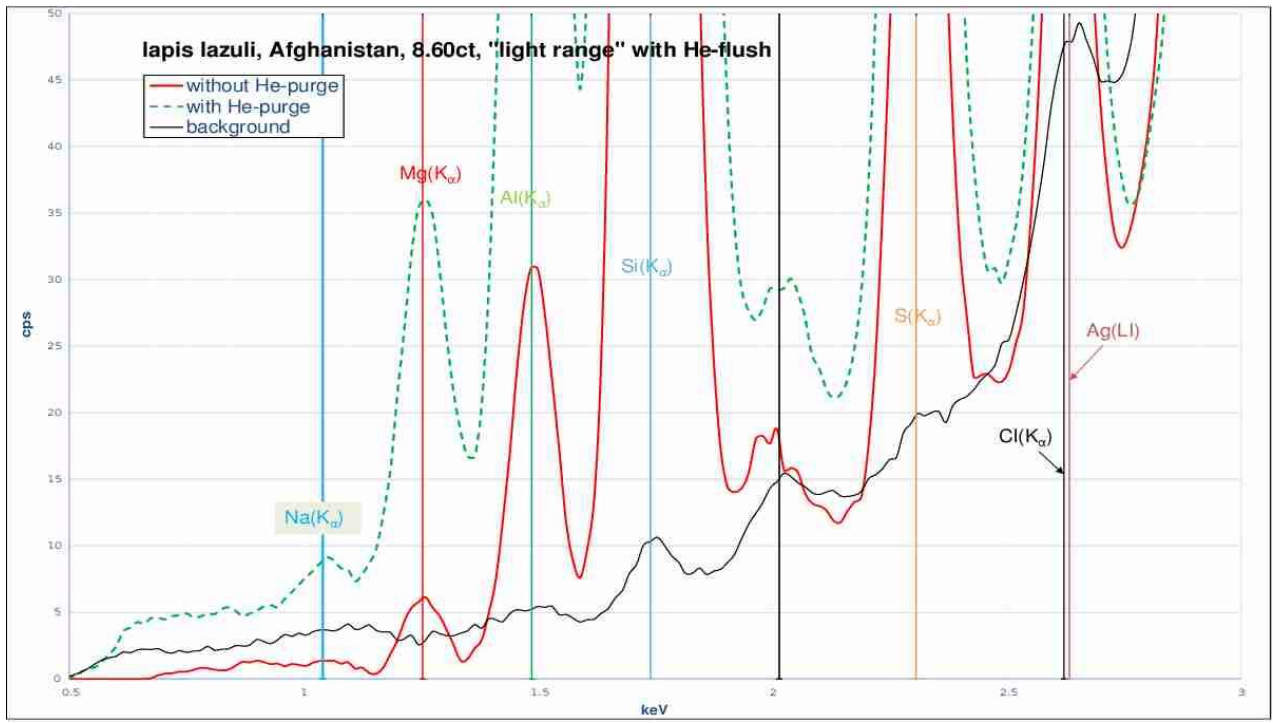
Figure DD-20: Lapis lazuli 'light range' spectra (enlarged version of Figure DD-19). The improvement in the detection of Na and Mg is remarkable when using the He purge unit.
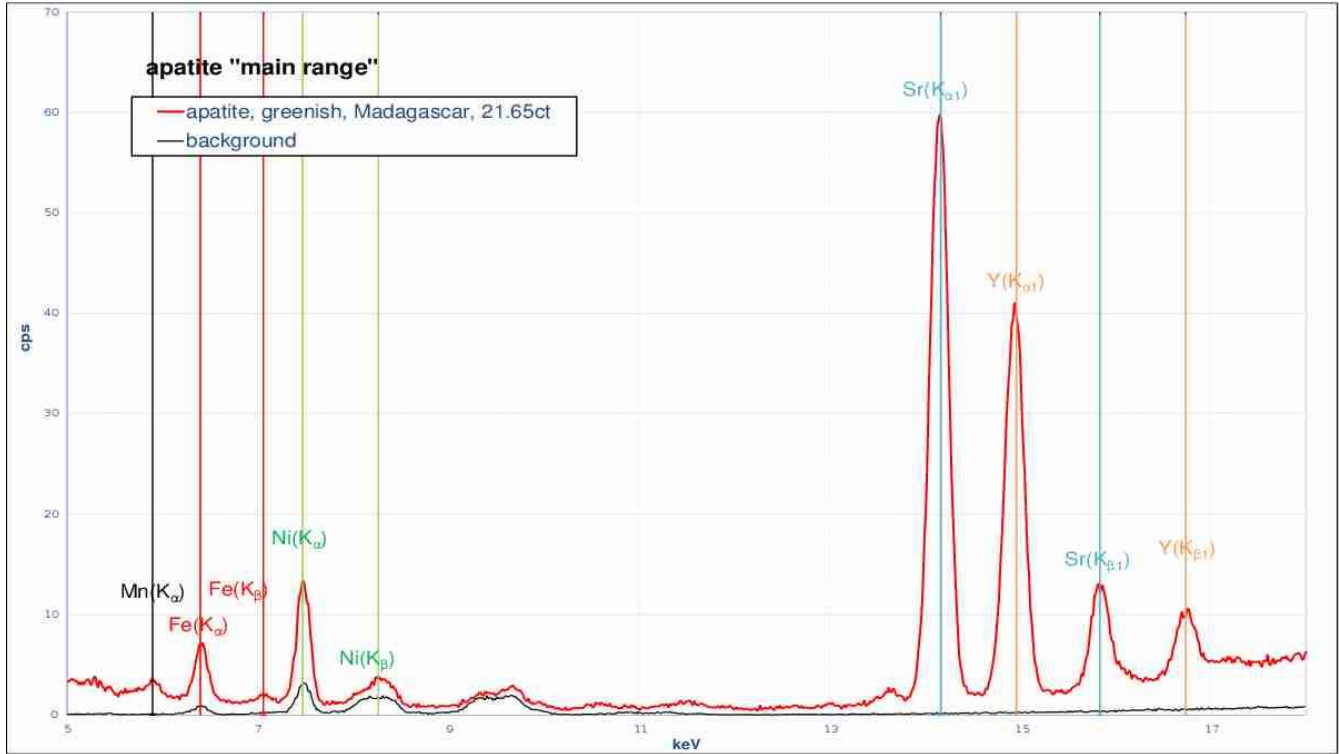
Apatite

Figure DD-21: 'Main range' spectrum of a greenish apatite from Madagascar (sample 17). Some of the Ca sites within apatite can be populated by Sr, which is quite clear in this spectrum. Apart from common REE contributions, this apatite also has clear Y signal.
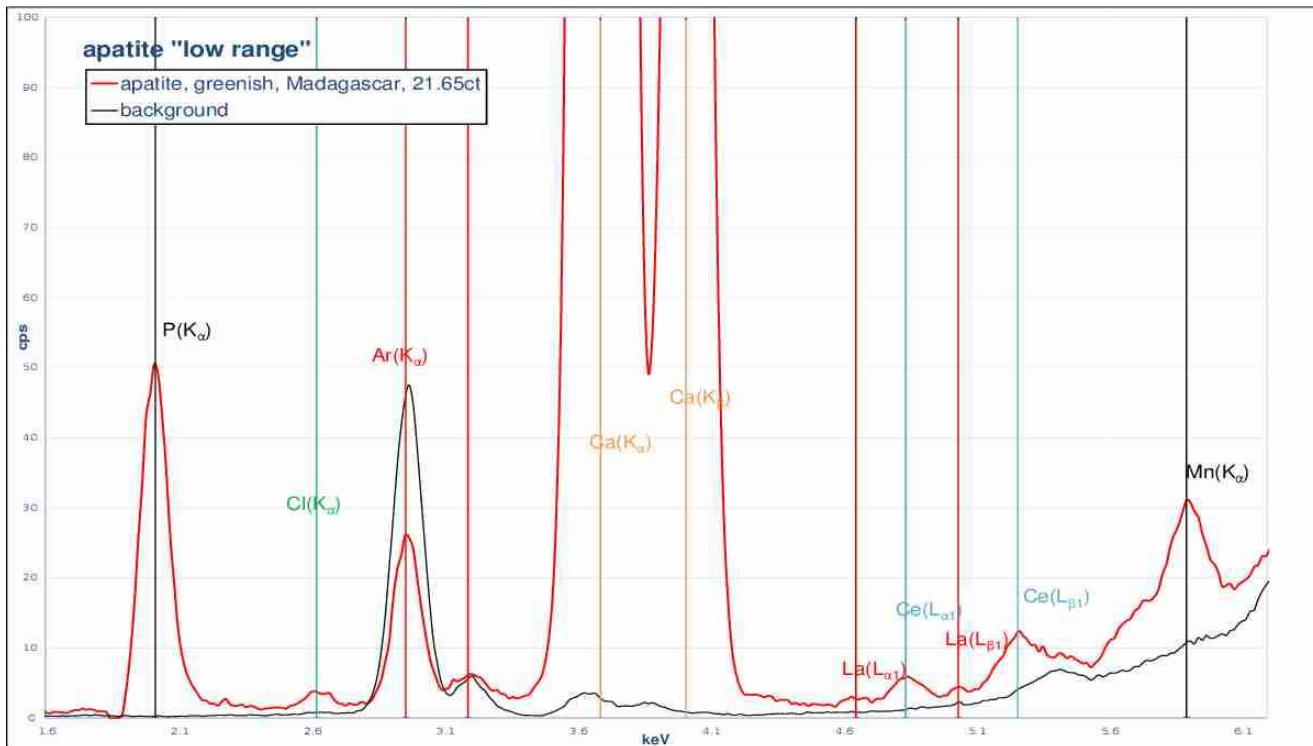
Figure DD-22: 'Low range' spectrum of the apatite shown in Figure DD-21. As apatite is a phosphate, a clear P peak is expected. This apatite apparently also has a small Cl component. REE are detectable by their L-lines (here, for La and Ce).
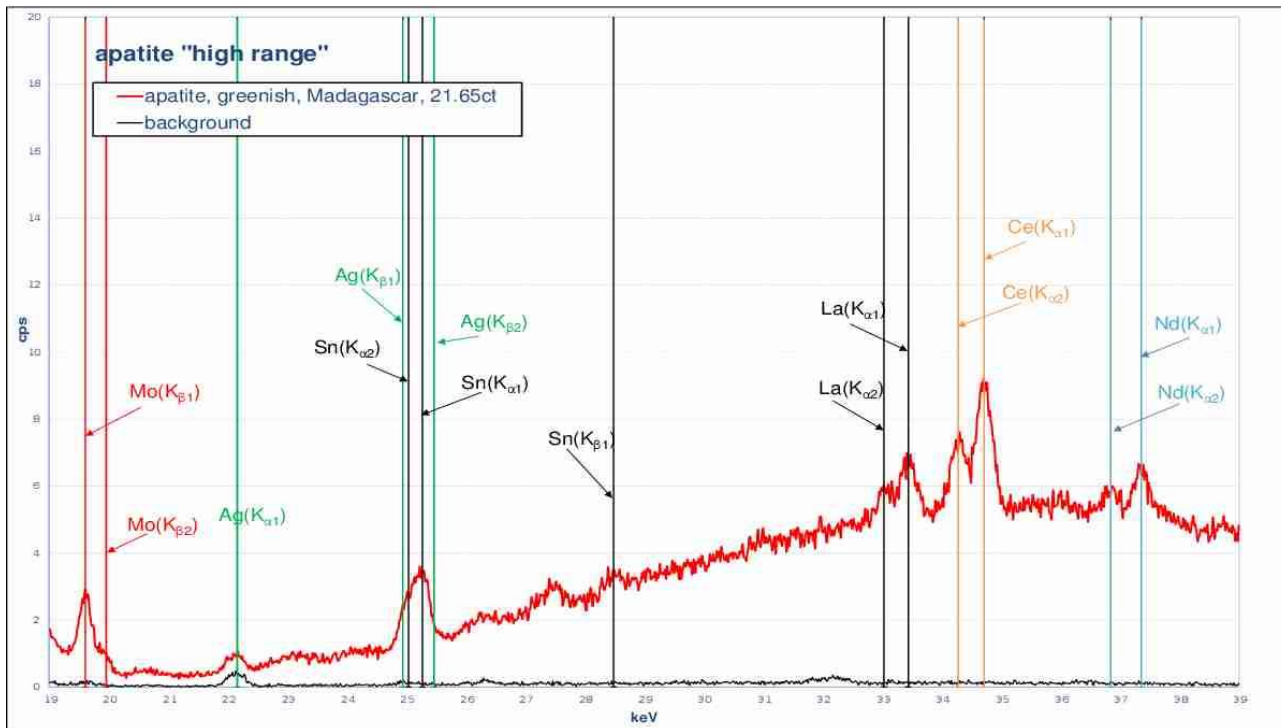

Figure DD-23: 'High range' spectrum of apatite (sample 17). The K-lines for REE are detectable within this energy range. Not only La and Ce can be seen, but also traces of Nd. Sn lines are also visible, and indeed the quantitative result calculated by the instrument showed the presence of Sn. (Sn is also a system peak.) The Ag and Mo lines are system peaks but their concentrations are statistically not significant.
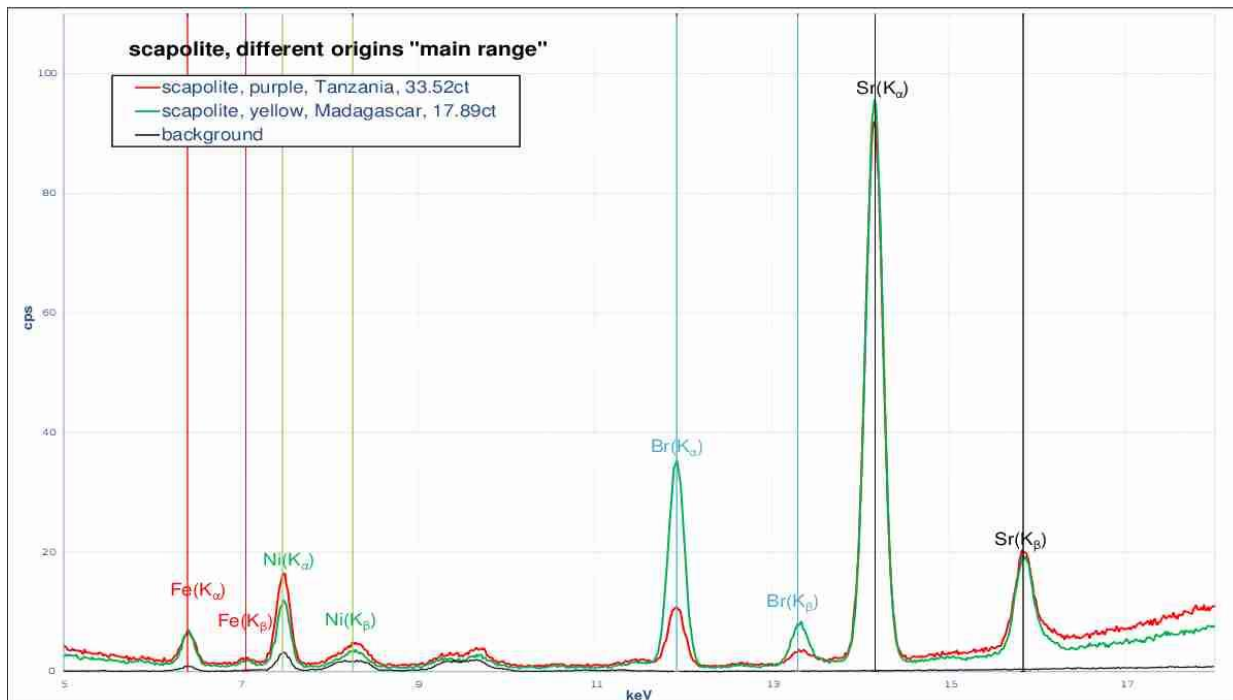
Scapolite

Figure DD-24: 'Main range' spectra of scapolites (samples 18 and 19). The author was at first surprised by the very clear Br signal, although this element is known in scapolite (Dong, 2005). Samples 18 and 19 are quite different in colour (yellow and purple), but no transition metal was found that could be responsible for that difference.
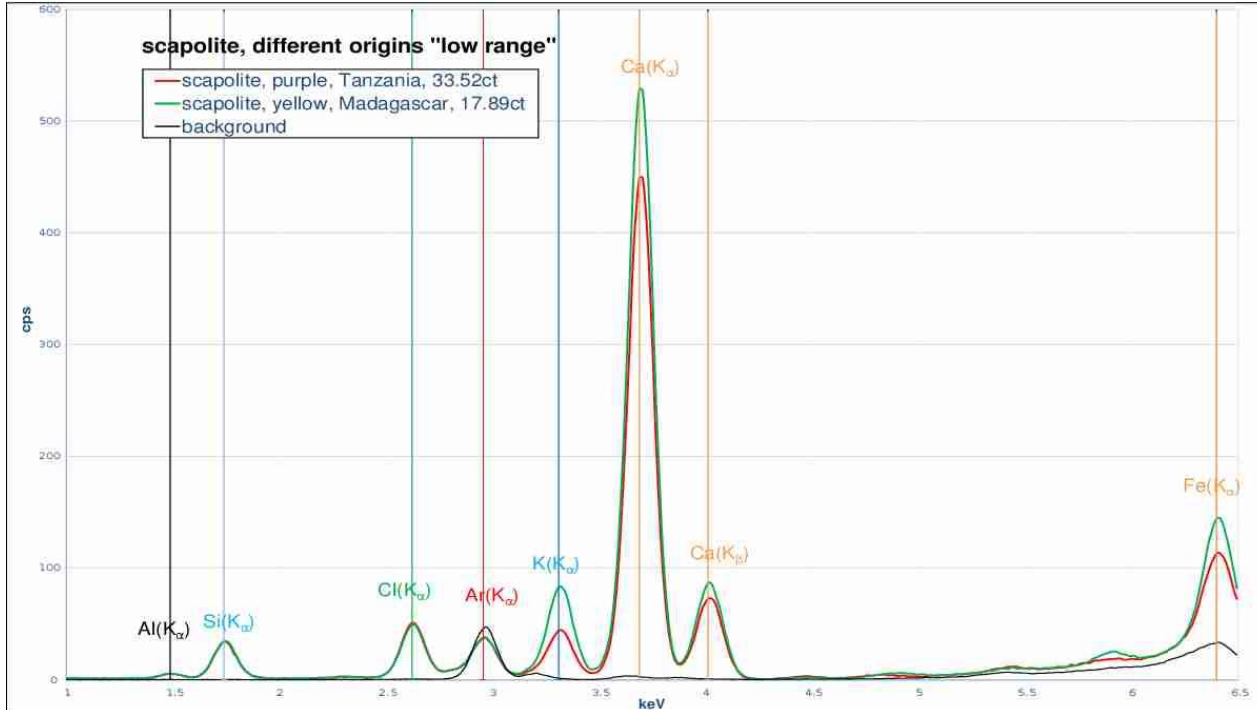

Figure DD-25: 'Low range' spectra of scapolites (samples 18 and 19). Scapolite is formed by the solid-solution series marialite and meionite ($Na_4Al_3Si_9O_{24}Cl$ to $Ca_4Al_6Si_6O_{24}CO_3$). To investigate the amount of each end-member, an analysis with the He-purge unit should be performed to improve the detection of Na. Both scapolites have a rather high alkaline earth content (Ca and Sr), and hence they have a clear meionite end-member contribution. The presence of Br as well as Cl show the existence of the marialite component as well.

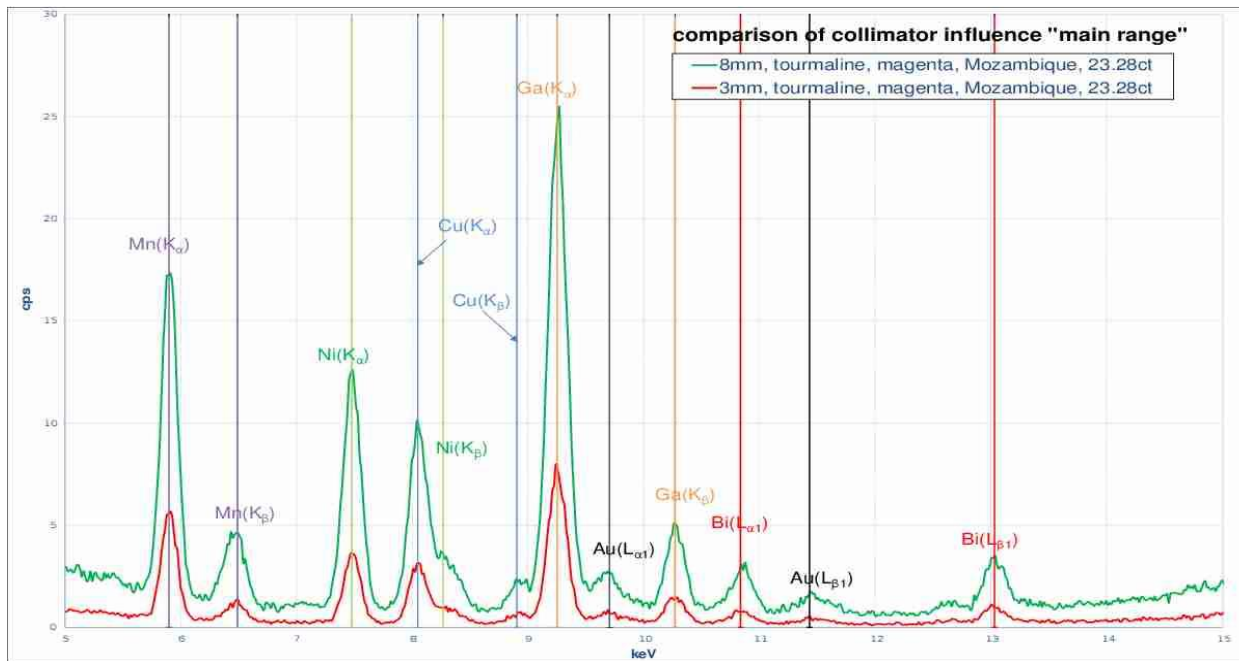**Comparison of Results from Different Collimators (3 and 8 mm)**

Figure DD-26: 'Main range' spectra of a Mozambique tourmaline (sample 20), measured with two different collimators (3 and 8 mm). The area probed by the 3-mm-collimated beam is much smaller and hence the fluorescence intensity of the peaks is weaker. Nevertheless, the pattern of the elements in the gem is still recognizable, and the stone can be identified as a Mn,Cu-bearing tourmaline with some Ga and Bi. The Ni system peak is strongly visible, but the Ni concentration was quantitatively given in both cases as 'LOD'.
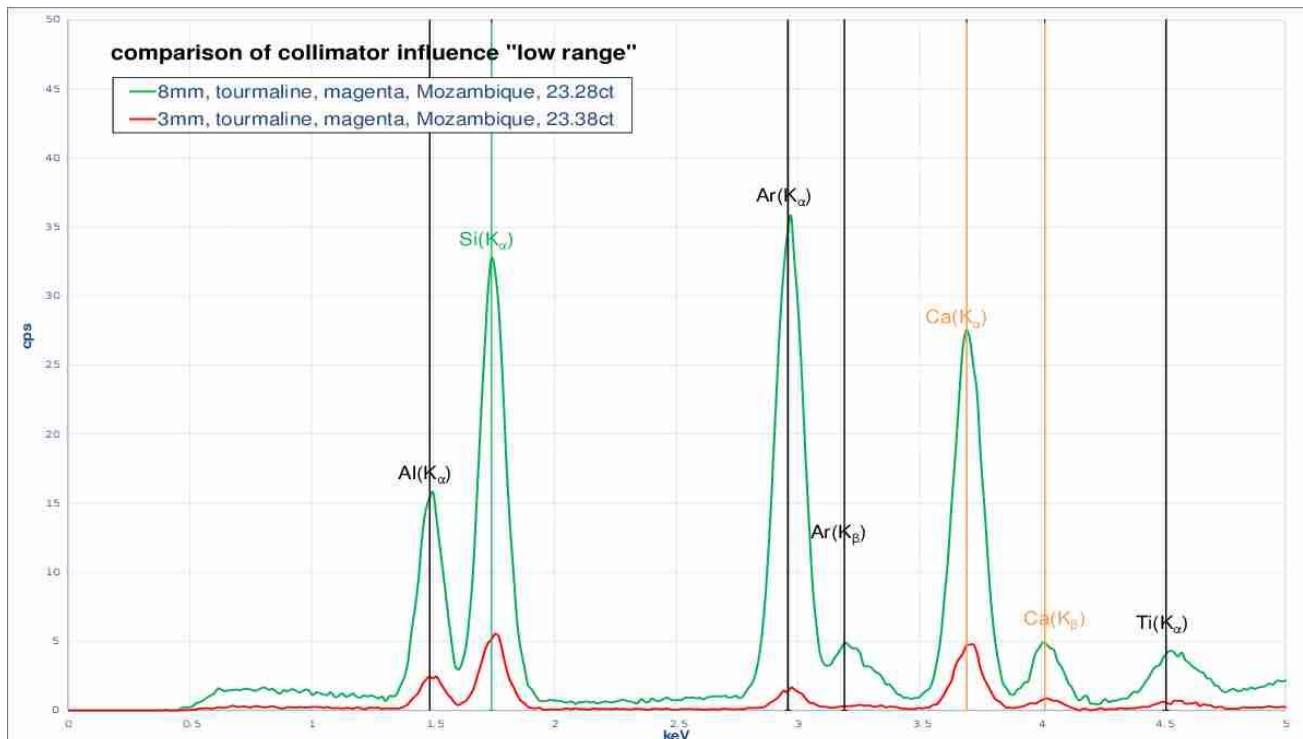

Figure DD-27: 'Low range' spectra of the sample in Figure DD-26 measured with 3 and 8 mm collimators. All the elements can be detected with the 3 mm collimator. In both cases a small liddicoatite component (Ca) can be seen.
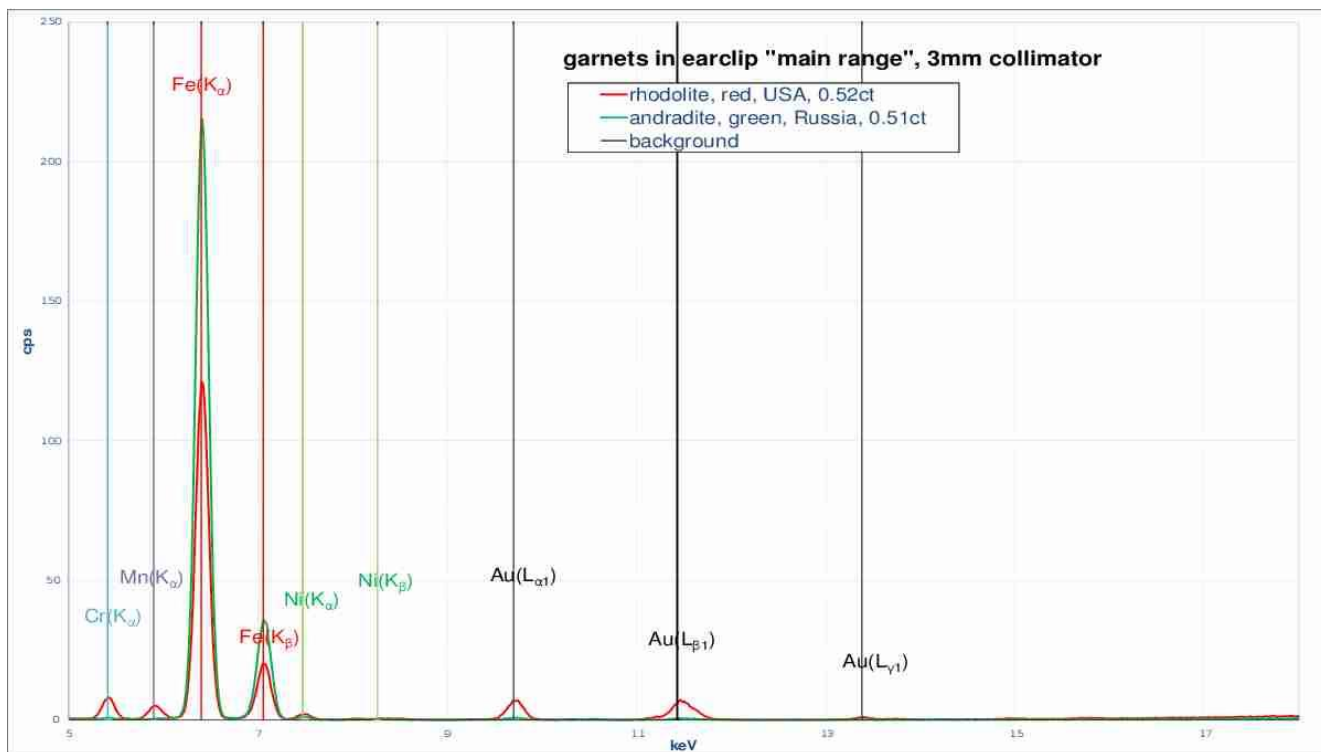
14

Analysing Mounted Gemstones

Figure DD-28: 'Main range' spectra of two garnets, each mounted in a gold setting (samples 21a and 21b). The two stones are small (3 mm in diameter). The colour-defining components of the rhodolite can be easily seen (Fe, Mn and Cr), as well as some Au from the mounting. For the andradite garnet, only Fe can be seen.
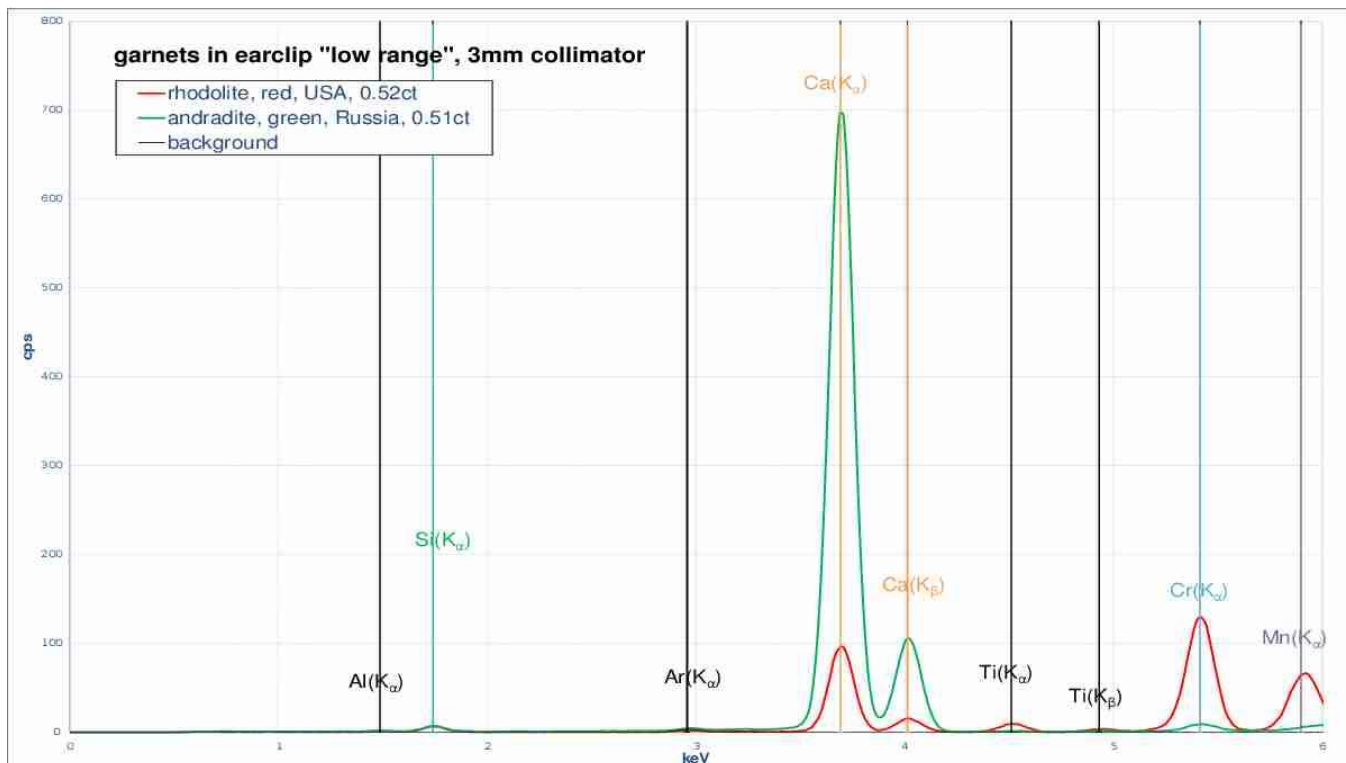

Figure DD-29: 'Low range' spectra of samples 21a and 21b. The Cr content of the andradite is quite low, but the colour of that stone would probably allow the name 'demantoid' without any doubt. There is a small grossular component (Ca) within the rhodolite.
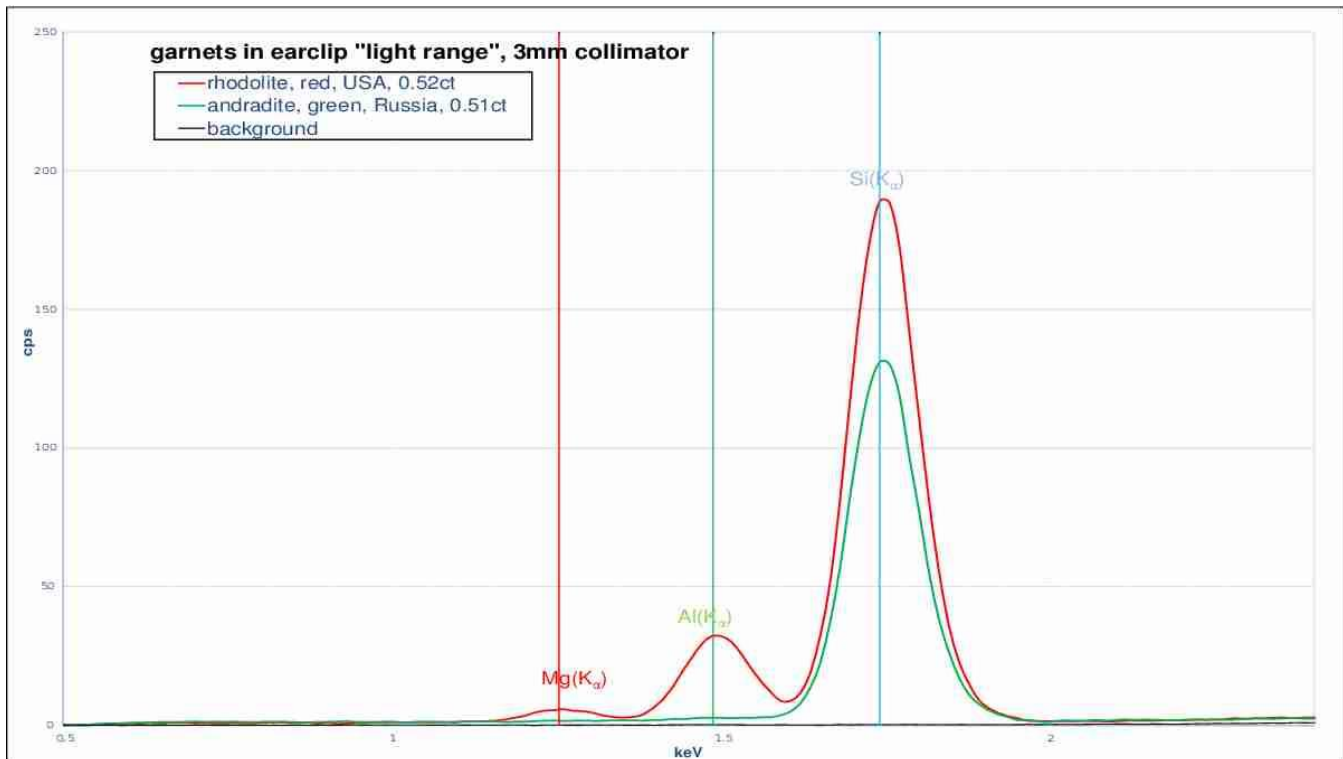
Figure DD-30: 'Light range' spectra of samples 21a and 21b. The pyrope component (Mg) of the rhodolite (sample 21a) is clear, as well as the absence of Al from an andradite (21b).

References

Dong P., 2005. Halogen-element (F, Cl and Br) behaviour in apatites, scapolite and sodalite: An experimental investigation with field applications. Ph.D. thesis, University of Saskatchewan, Saskatoon, Canada.

Hänni H.A., 1982. A contribution to the separability of natural and synthetic emeralds. *The Journal of Gemmology*, **18**(2), 138–144, http://dx.doi.org/10.15506/jog.1982.18.2.138.

Nassau K., 1980. *Gems Made by Man*. Gemological Institute of America, Santa Monica, California.